LANGMUIR Article
Cite This: Langmuir 2018, 34, 10333−10339
pubs.acs.org/Langmuir

Diffusion of Proteins across Silica Colloidal Crystals

Patricia Anne A. Ignacio-de Leon,† Yulia Eygeris, Robert Haynes, and Ilya Zharov*

Department of Chemistry, University of Utah, 315 S 1400 E, Salt Lake City, Utah 84112, United States

ABSTRACT: We studied the diffusion of three model proteins, lysozyme (Lz), bovine hemoglobin (BHb), and bovine serum albumin (BSA), normal to the (111) plane of sintered silica colloidal crystals with three different pore "radii" (7.5, 19, and 27 nm). We demonstrated that these colloidal crystals exhibit size selectivity when the nanopores are sufficiently small (7.5 and 19 nm). Because these nanopores are still larger than the diffusing proteins, the observed size selectivity can be attributed to the tortuosity of the colloidal nanopores. Larger (27 nm) nanopores led to higher transport rates but at the cost of selectivity. In addition to the size selectivity, we also demonstrated that 19 nm nanopores possess shape selectivity for the proteins of comparable molecular weights. We showed that the high temperature sintering required for the preparation of sintered colloidal crystals reduces the extent of interactions between the proteins and the nanopore surface, which appear to play a minor role in the diffusion, and that transport selectivity is decided solely by protein size and shape. Taken together, our observations suggest that sintered silica colloidal crystals constitute promising nanoporous membranes for protein separations, with easily controllable pore size, size and shape selectivity, and minimal surface fouling.

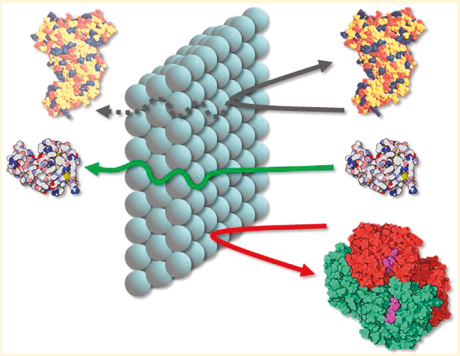

INTRODUCTION

Silica colloidal crystals comprise a close-packed face-centered cubic (fcc) lattice of silica spheres of submicrometer diameter, formed by self-assembly of the spheres. The tetrahedral and octahedral voids present in the close-packed system constitute ordered arrays of three-dimensional interconnected nanopores.[1] Originally, silica colloidal crystals have been developed as templates for the preparation of photonic[2] and magnetic materials,[3] macroporous polymer membranes,[4] and sensors.[5] However, they also constitute attractive inorganic nanoporous materials whose pore size can be readily controlled by the silica sphere size in the 10−100 nm range. Membranes with nanopores of this size are attractive for applications in food industry and water purification[6] as well as in separations of nanoparticles[7] and proteins.[8] Membrane separations provide considerable economic, environmental, and operational advantages[9] over traditional separation methods such as electrophoresis and chromatography.[10−14]

Presently, polymeric membranes are the most common type of membranes used in separations, especially those in biotechnology.[15] These membranes can be prepared using straightforward methods such as interfacial polymerization, phase inversion, or layer-by-layer assembly.[16,17] They offer adjustable pore size and charge, but irregular pore shape and size, defects, and inferior stability may limit their utility. However, these properties can be improved using block copolymer membranes that possess very uniform pores and are suitable for highly selective separations.[18]

Inorganic nanoporous membranes provide attractive alternatives for porous polymeric membranes because of their well-defined pore geometry and chemical, thermal, and mechanical robustness. Inorganic membranes can be prepared through condensation (zeolites[19] and metal−organic frameworks (MOFs)[20]), nanofabrication (e.g., in silicon nitride[21]), etching (porous silicon[22] and anodized alumina[23]), templating (mesoporous silica[24]), and controlled growth (graphene[25] and carbon nanotubes[26]). Despite many advances in the field of inorganic nanoporous membrane materials, several problems remain unsolved including low pore density, difficulty varying pore size in a broad range and high thickness resulting in low separation speed. In addition, many of these membrane materials require specialized methods for their preparation.

Novel approaches to the preparation of nanoporous membranes recently involved self-assembly of nanoparticles.[27] In particular, silica colloidal membranes, developed in our group,[28] provide a simple and powerful self-assembly approach to inorganic nanoporous membranes that possess the following superior properties: (1) nanopore size easily variable in a broad range,[29] (2) high molecular flux, and (3) facile surface chemistry.[30] Silica spheres used in the assembly of colloidal crystals are easily produced by a sol−gel reaction,[31] and the self-assembly process is well developed.[29] The ease with which the nanopore size in silica colloidal membranes can be tailored for a given application is particularly important.

Previously, we demonstrated that silica colloidal crystals, in the form of thin films, possess high ionic transport selectivity when their surface is modified with charged moieties such as amines,[32,33] sulfonic acid groups,[34,35] and spiropyran molecules,[36] due to electrostatic interactions of the diffusing species with the nanopore surface. Alternatively, surface modification

Received: April 17, 2018
Revised: July 4, 2018
Published: August 7, 2018

DOI: 10.1021/acs.langmuir.8b01261
Langmuir 2018, 34, 10333−10339

of the nanopores with neutral moieties, such as chiral selectors[37,38] and thiacalixarenes,[39] allows achieving high selectivity for molecular transport using molecular recognition mechanisms. We showed that transport selectivity in silica colloidal crystals can be achieved even in the case when the nanopore size is significantly larger than the diffusing species, and that this is the result of the high surface area and tortuosity of the silica colloidal crystals.[28]

In order to apply silica colloidal membranes in separations, we developed free-standing silica colloidal crystals.[40] These materials were prepared by sintering, which causes the silica spheres to fuse to one another[41,42] and provides defect free, mechanically robust colloidal crystals with flexural strength of 49 ± 9 MPa.[40] Earlier, we showed that sintered silica colloidal membranes possess size selectivity for the transport of synthetic macromolecules.[43] In that work, we used Rhodamine B isothiocyanate-labeled polyamidoamine (PAMAM) dendrimers as diffusion probes due to their high monodispersity, well-defined molecular architecture and size ranging from 2 to 20 nm. We found that while generation-2 dendrimer diffused about three-fourths as fast as generation-1 through the membranes prepared from 100 nm silica spheres (7.5 nm "radius" pores), generation-3 had a diffusion rate ca. 3 times lower and generation-4 and generation-5 had roughly the same diffusion rates, about four times lower than that of generation-1. This is noteworthy considering that there is only about 3−4 nm difference between the diameters of generation-4 and generation-5 and of generation-1 dendrimers, and that the size of the colloidal nanopores is significantly larger than the dendrimer diameter, suggesting an additional effect of tortuosity on the size selectivity. In addition, we observed that the generation-5 dendrimer diffused at slightly higher rate than the generation-4 dendrimer. As the size of the generation-5 dendrimer is larger, this increase in diffusion rate was related to the increased flexibility of the generation-5 dendrimer.

Given the attractive separation properties of silica colloidal crystals in the case of small molecules and synthetic macromolecules, it was important to investigate their utility for protein separations. Indeed, the ability to separate proteins is crucial in medical, biological and pharmaceutical research and also in clinical diagnosis.[44] For example, detection of proteins with low natural abundance in the presence of highly abundant proteins remains one of the biggest challenges in proteomics.[45] Separation of similar size proteins is another common problem.[46] Thus, systems capable of fast and selective protein transport would be extremely useful for protein purification and analysis, including applications in single molecule biosensors[47,48] and sample preconcentration for nanofluidic devices.[11] While close-packed silica colloidal systems have been used in liquid chromatography separations of proteins,[49,50] silica colloidal crystal membranes have not been explored for protein separations.

In order to evaluate the utility of sintered silica colloidal membranes in protein separations, we studied the diffusion of model proteins though these materials with three different nanopore sizes. We selected three model proteins: lysozyme (Lz), bovine hemoglobin (BHb), and bovine serum albumin (BSA), for our studies as they vary in isoelectric point, size, and shape (Table 1). In this study, we considered the effects of the pore size and the surface properties and protein adsorption.

Table 1. Characteristics of the Proteins Used

	mass (kDa)	dimensions (nm)	Stokes radius (nm)	pI
Lz	14	3.2	2.0[13]	11.4
BHb	65	6.4 × 5.5 × 5	3.2[39]	7.1
BSA	67	4 × 4 × 14	3.6[13]	4.8

EXPERIMENTAL SECTION

Materials. Ammonium hydroxide (28−30% as NH_3, EMD Chemicals, Inc.), potassium phosphate monobasic (Sigma), potassium phosphate dibasic trihydrate (Mallinckrodt), tetraethylorthosilicate (TEOS, 99.999+%, Alfa Aesar), lysozyme (from chicken egg white, Sigma), albumin (from bovine serum, lyophilized powder, Sigma), hemoglobin (from bovine blood, lyophilized powder, Sigma), ethanol (200 proof, ACS-grade, Pharmaco-Aaper), and methanol (ACS Reagent, Sigma-Aldrich) were all used as received. Deionized water (18 MΩ·cm) used in all experiments was obtained from a Barnstead "E-pure" water purification system.

Instrumentation. Scanning electron microscopy (SEM) images were obtained using either a Hitachi S3000-N or an FEI NanoNova instrument. Transmission electron microscopy (TEM) images were obtained using an FEI Philips Tecnai T-12 instrument. UV/vis measurements were collected using an Ocean Optics USB2000 or USB4000 instrument. A Branson 1510 sonicator was used for all sonications. A Clay Adams Compact II Centrifuge (3200 rpm, Becton Dickinson) was used for all centrifugations. A Fisher Scientific Isotemp Programmable Muffle Furnace (model 650) was used for calcination and sintering. Dynamic light scattering (DLS) and zeta-potential measurements were carried out using a NICOMP 380 ZLS Zeta Potential/Particle Sizer (PSS NICOMP Particle Sizing Systems).

Preparation of Silica Spheres. Three batches of silica spheres with varying sizes (Table 2) were prepared as described earlier.[31] The size of the spheres was controlled by the preparation conditions as follows: [TEOS] = 0.2 M, [NH_3] = 0.4 M, [H_2O] = 16.0 M, 25 °C for 24 h gave 260 ± 30 nm particles (measured by DLS), [TEOS] = 0.2 M, [NH_3] = 1.1 M, [H_2O] = 17.0 M, 25 °C for 24 h gave 388 ± 30 nm particles (measured by DLS), and [TEOS] = 0.2 M, [NH_3] = 4.0 M, [H_2O] = 5.0 M, 10 °C for 6 h gave 444 ± 40 nm particles (measured by DLS). The silica spheres were then calcinated at 600 °C for 4 h, and their sizes were determined using SEM from 100 individually measured spheres to be 231 ± 20, 350 ± 20, and 427 ± 30 nm in diameter, respectively.

Preparation of Silica Colloidal Crystals. The free-standing silica colloidal crystals were prepared by first vertical deposition of ∼12 wt % colloidal solutions of calcinated silica spheres (260 ± 30, 388 ± 30, and 444 ± 40 nm diameter) in ethanol onto a glass substrate. The resulting colloidal crystals were then gently lifted from the substrate and sintered in a furnace for 12 h at 1050 °C (desired temperature achieved at a heating rate of 20 °C/min).[51] SEM images (Figure 1) of these crystals were obtained to give average silica sphere diameters of 100 ± 6, 252 ± 10, and 362 ± 27 nm, respectively, as measured from 100 individual spheres in each colloidal crystal. The thickness of each colloidal crystal was measured with a Vernier caliper at six different points throughout the piece, giving the average thickness of ∼200 μm. The colloidal crystals possessed ∼1 cm^2 area.

Diffusion Measurements. To prepare membranes suitable for diffusion measurements, sintered colloidal crystals were sandwiched between two PTFE washers (5.0 mm inner diameter, 14.0 mm outer diameter and 1.0 mm thickness, Small Parts, Inc.) with Loctite Hysol 0151 Epoxy and allowed to cure for at least 24 h prior to use for diffusion experiments (Figure 2). Diffusion experiments were performed by placing a membrane between two connected 1 cm quartz cuvettes. The feed cell contained 4.00 mL of a pH 6 10 mM phosphate-buffered aqueous 0.025 mM protein solution while the reservoir cell contained 4.00 mL of the 10 mM buffer solution. The membranes were placed between two Kalrez o-rings to guard against leaking, and the assembly was then secured with a clamp. Each cell was covered with Parafilm to prevent eventual evaporation, and the contents of both cells were continually stirred. The reservoir cell was

DOI: 10.1021/acs.langmuir.8b01261
Langmuir 2018, 34, 10333−10339

Table 2. Summary of Measured Diameters for the Silica Nanoparticles and the Corresponding Assemblies

as made		calcinated		sintered	
DLS	SEM	DLS	SEM	SEM	pore "radius"
260 ± 30	261 ± 20	239 ± 30	235 ± 20	100 ± 6	7.5
388 ± 30	[a]	359 ± 30	346 ± 20	252 ± 10	18.5
444 ± 40	432 ± 30	418 ± 30	427 ± 30	362 ± 30	26.6

[a]Data not collected.

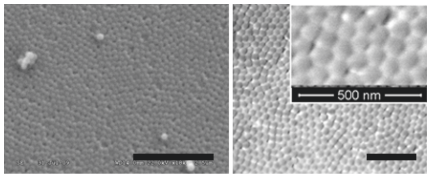

Figure 1. SEM images of a sintered colloidal crystal made from 235 nm (calcinated) silica spheres. (Left) Low magnification image (scale bar 2.5 μm) showing that there are no major cracks or defects in the sample. (Right) High-Resolution image (scale bar 500 nm) and inset that shows adjacent spheres fused at contact points.

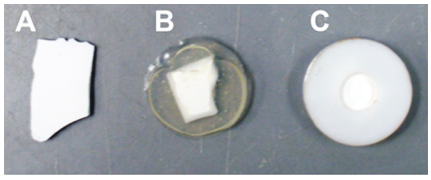

Figure 2. Photographs of sintered colloidal crystal: (A) as prepared, (B) imbedded in epoxy resin, and (C) with PTFE washers. Scale bar is 1 cm.

placed between two fiber optic cables. The flux was monitored by recording the absorbance in the reservoir cell for at least 12 h (Figure 3). In diffusion experiments with a mixture of two proteins in the feed

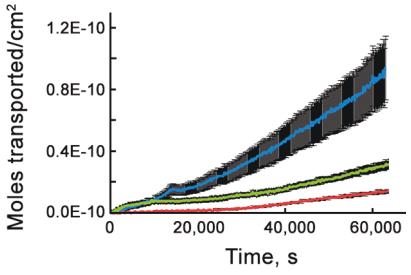

Figure 3. Transport of Lz (blue), BHb (red), and BSA (green) across sintered colloidal crystals with 19 nm pore "radius".

cell, the absorbances at both λ_{max} values for Lz, BSA and BHb (280, 277, and 499 nm, respectively) were simultaneously recorded. Data points were acquired every 150 s with an initial delay of 150 s. Prior to using a membrane for a new trial, it was immersed in buffer for at least 2 days and the solution replaced occasionally to ensure removal of any previous probe molecules from within the colloidal crystal.

Determination of the Extent of Protein Adsorption. Calcinated silica spheres (0.035 g) were dispersed into 6.0 mL pH 6 10 mM phosphate buffer and the colloidal solution was then divided into three 2 mL aliquots. Individual solutions (0.025 mM) of Lz, BSA, and BHb were prepared in the same buffer, and 2.0 mL of each was added separately to an aliquot of unmodified and modified silica followed by incubation for 24 h with gentle stirring at ambient conditions. The mixtures were centrifuged and the UV−vis absorbance was recorded for each of the supernatants.

RESULTS AND DISCUSSION

Preparation and Geometry of Sintered Colloidal Crystals. Silica colloidal crystals can be easily prepared by deposition from solution; however, the resulting crystals are quite fragile and need a solid support such as glass to prevent disintegration. To prepare free-standing colloidal crystals, we sintered the silica spheres at 1050 °C, which fused the surfaces of the adjacent spheres at contact points via Si−O−Si bonds. The silica spheres had to be calcinated at 600 °C prior to colloidal crystal assembly to ensure the complete removal of solvent (water and ethanol) that remains trapped within the silica network. The calcination produced denser spheres as evidenced by the decrease in their diameter as measured by both DLS and SEM (Table 2). This calcination was reported to prevent the formation of cracks within the membrane upon sintering at further elevated temperatures.[51] Sintering led to even greater decreases in the sizes of the spheres, while maintaining the overall fcc-packed structure, as we demonstrated earlier.[40] It appeared that smaller spheres experienced greater reductions in size, presumably due to their larger surface area-to-volume ratio compared to bigger spheres. Spheres with diameter of 235 nm decreased in size by 57.4% to yield membranes composed of 100 nm spheres; 345 nm spheres decreased by 27.0% to 252 nm, while 427 nm spheres decreased by only 15.2% to a diameter of 362 nm. The now robust free-standing colloidal crystals were then prepared for diffusion experiments by sandwiching a piece between two washers using an epoxy resin as adhesive (Figure 2).

Figure 1 shows an SEM image of a colloidal crystal sintered at 1050 °C and demonstrates the absence of any major defects over a large area. Occasional point defects within the fcc lattice were present but did not seem to persist beyond one or two layers. Previously, we demonstrated, using flux and diffusion measurements, that sintered colloidal crystals do not contain mechanical defects.[40]

Diffusion of Proteins through Sintered Silica Colloidal Crystals. To determine whether size-selective transport of proteins based on the difference in their size relative to nanopore "radius"[47] could be achieved with the sintered silica colloidal crystal, we studied the diffusion of common model proteins. Lz, BHb, and BSA were chosen for their availability, size, and shape range (Table 1), and abundance of reports describing their diffusion behavior.[52−56] Comparison of their diffusion rates would provide information about the pore selectivity as the sizes of the proteins are varied; while comparison of BHb and BSA would afford insight into the effect of the shape of the protein on the diffusion through the nanopores (BHb is roughly spherical whereas BSA has an ellipsoid shape).

The diffusion rate R_D (mol·s^{-1}) through a colloidal crystal membrane of known thickness L and area S was determined by measuring the amount of a protein that diffused through the membrane as a function of time. Knowing the value of R_D

DOI: 10.1021/acs.langmuir.8b01261
Langmuir 2018, 34, 10333−10339

Table 3. Protein Diffusion Coefficients D_{col} (cm^2/s) through Sintered Colloidal Crystals and Corresponding Selectivities

		19 nm pore				7.5 nm pore		27 nm pore	
protein	Stokes correction	D_{col} at pH 6, $cm^2/s \times 10^{-7}$	selectivity relative to Lz	D_{col} at pH 4, $cm^2/s \times 10^{-7}$	selectivity relative to Lz	D_{col} at pH 6, $cm^2/s \times 10^{-7}$	selectivity relative to Lz	D_{col} at pH 6, $cm^2/s \times 10^{-7}$	selectivity relative to Lz
Lz	1.0	2.99 ± 0.10		2.82 ± 0.27		0.82 ± 0.19		2.3 ± 0.6	
BHb	0.625	0.81 ± 0.07	2.3	0.83 ± 0.05	2.1	no diffusion		1.33 ± 0.2	1.1
BSA	0.556	1.43 ± 0.34	1.2	1.49 ± 0.20	1.1	0.08 ± 0.01	5.7	1.28 ± 0.1	1.0

allowed for the calculation of the molecular flux J_{col} ($mol \cdot s^{-1} \cdot cm^{-2}$) through the colloidal crystal (eq 1).

$$R_D = J_{col} S \tag{1}$$

A solution of Fick's law for diffusion (eq 2) was then used to calculate the diffusion coefficients D_{col} ($cm^2 \cdot s^{-1}$) of the proteins as they traversed across the colloidal crystal.[57]

$$J_{col} = \frac{\Delta C}{L} D_{col} \tag{2}$$

While colloidal crystals contain nanopores of two sizes, when prepared by vertical deposition of silica spheres and used as thin membranes, the molecular transport through colloidal crystals occurs normal to the (111) plane of the fcc-packed structure. Thus, molecules enter the crystal through the concave triangular openings between the silica spheres. Octahedral pores found in the (100) direction of the colloidal crystal are much larger, and thus the smaller nanopores determine the size selectivity of the system, which we demonstrated previously in several systems.[28] Earlier, we also demonstrated[58−61] that the size of these openings can be estimated with reasonable accuracy as the distance from the center of their projection to the nearest sphere surface. The validity of this estimate was confirmed by others using simulations.[62] This distance, which we will call the pore "radius", is ca. 15% of the silica sphere radius.[63] Thus, colloidal crystals composed of 100, 252, and 362 nm spheres have nanopores whose centers are 7.5, 19, and 27 nm, respectively, away from the nearest silica sphere surface.

We first investigated sintered silica colloidal crystals with 19 nm pore "radius". Figure 3 shows the transport of the three proteins studied while Table 3 summarizes the calculated D_{col} values. These values are in good agreement with those predicted based on aqueous solution diffusion coefficients reported for Lz (~$2.2-2.8 \times 10^{-6}$ cm^2/s[64,65]), BHb, and BSA(~$0.6-0.8 \times 10^{-6}$ cm^2/s[66,67]) by taking into account the void fraction of fcc-packed structure ($\varepsilon = 0.26$[1]) and its tortuosity ($\tau = 3.0$[63]), which affect the diffusion coefficient as $D_{col} = (\varepsilon/\tau)D_{sol}$.[63]

We found that there was a general trend of decreasing diffusion coefficients with increasing size of the diffusing species. Lz diffused 3.7 and 2.1 times faster than BHb and BSA, respectively (Table 3). The observed difference in diffusion coefficients may be due to the interactions of the proteins with the tortuous nanopores of the colloidal crystals or due to the difference in Stokes radii between the diffusing proteins. In order to distinguish between these two factors, we used the Stokes−Einstein equation ($D_{sol} = kT/6\pi\eta R$, where R is solute radius). This equation can be rearranged to give an estimate of the relative diffusion rates of the proteins, $D_{sol}^{(1)}/D_{sol}^{(2)} = R^{(2)}/R^{(1)}$, assuming similar viscosities for the 0.025 mM protein solutions in water.[68] Thus, using the Stokes radii of the proteins (Table 1),[68,69] the Stokes−Einstein equation predicts that, in free solution, the diffusion coefficient of BHb would be 0.625 of that of Lz, while the diffusion coefficient of BSA would be 0.556 of Lz. Using these Stokes radius correction factors, we calculated (eq 3) the selectivity of the colloidal crystal membranes for the diffusion of the model proteins relative to Lz.

$$\text{selectivity} = \frac{D_{col}}{D_{col}(\text{Lz})} \times (\text{Stokes corr}) \tag{3}$$

Selectivity of unity would correspond to the difference in diffusion rates resulting solely from the difference in Stokes radii, while selectivity values higher than unity would indicate hindered transport of the proteins within the nanopores. We calculated the selectivity of 2.3 for BHb and 1.2 for BSA, which means that 19 nm colloidal nanopores provide size selectivity despite the fact that these nanopores are significantly larger compared to the sizes of the diffusion probes. This is similar to our earlier observations of high transport selectivity for both small and macromolecules in silica colloidal crystals, which we explained based on the tortuosity of the colloidal nanopores.[43] Furthermore, while BSA was expected to diffuse slower than BHb based on its Stokes radius, D_{col}(BSA) was 1.8-fold higher than D_{col}(BHb) (2-fold if taking into account the Stokes radius correction). It appears that the prolate ellipsoid shape of BSA may allow traversing more readily through the nanopores compared to the more spherical BHb despite their similar molecular weights (Table 2). This is similar to our earlier observations for higher diffusion rate of larger but more flexible dendrimers through colloidal nanopores.[43] Thus, colloidal crystals with 19 nm "radius" pores show both size-selective transport as well as shape-selectivity for model proteins.

Next, we prepared colloidal crystals with smaller spheres leading to the nanopore "radius" of 7.5 nm, which allowed investigating how protein transport is affected by the pore size. It is apparent (Table 3) that D_{col} for all diffusing species were greatly reduced. Size selectivity was expected to improve as the nanopores became narrower until a point where complete blockage occurred as the nanopore became too small to accommodate a diffusing species. Given that the diameters of Lz and BSA are smaller than the 7.5 nm nanopore "radius", it was not surprising that complete blockage for these proteins was not observed. However, the diffusion rates for Lz and BSA were reduced 3.6- and 18-fold, respectively, whereas a cutoff was observed for the bulkier BHb. The use of the smaller nanopores led to improved selectivity of 5.7 for Lz over BSA and also suggested that a complete separation of a mixture of BHb and BSA could be achieved.

Finally, silica colloidal crystals with a larger nanopore "radius" (27 nm) were prepared and D_{col} values for the model proteins were measured (Table 3). Generally, transport rates through the pores of increased diameter were comparable to those observed for 19 nm "radius" pores. However, as expected[68] for these wide 27 nm pores, the rates of transport were in the order of Lz > BHb ≈ BSA due to the Stokes radii differences, and transport selectivity was not observed.

DOI: 10.1021/acs.langmuir.8b01261
Langmuir 2018, 34, 10333−10339

In an effort to further evaluate the separation capabilities of sintered silica colloidal membranes, we performed two-species diffusion experiments for 1:1 mixtures of Lz/BHb and BSA/BHb. Membranes with 19 nm "radius" were able to enrich the permeate with Lz compared to BHb by a factor of 4, somewhat higher compared to that predicted based on the diffusion coefficients. This maybe the result of the competitive diffusion inside the nanopores. The permeate of the BSA/BHb mixture was enriched with BSA by a factor of 1.5, slightly lower than that predicted based on their respective diffusion coefficients. Membranes with 7.5 nm "radius" were able to completely separate the Lz/BHb and the BSA/BHb mixtures.

Protein Interactions with Nanopore Surface. Silica possesses a negative surface charge due to the presence of the silanol (Si−OH) groups.[9] At pH 6, Lz and BHb are both cationic according to their pI values (Table 1) with Lz bearing at least +8 charge[53] attributed to six lysine residues.[70] On the other hand, BSA is anionic at pH values beyond its pK_a of 4.7.[44]

In order to evaluate the potential electrostatic effects for the diffusion of the model proteins through silica colloidal nanopores, we measured the diffusion rate at pH 4, where all proteins are positively charged. We did not observe any significant change in the diffusion rates under these conditions. Furthermore, we increased the ionic strength of the solution by using a 100 mM phosphate buffer, and also did not observe any changes in the diffusion rates. This suggests that electrostatics does not play a significant role in the diffusion of the proteins across sintered colloidal crystals. This may be due to the high temperature calcination and sintering processes used. It is known that heat treatment of silica at temperatures higher than 300 °C results in dehydroxylation of the existing Si−OH groups and the formation of Si−O−Si groups accompanied by the decrease in the surface negative charge, with treatment above 1000 °C resulting in permanent and almost complete removal of the silanol groups.[71,72] The latter should be accompanied by a further decrease in the surface negative charge compared to that observed for the calcinated silica spheres, which in turn should lead to weaker electrostatic interactions of the model proteins inside the nanopores. In order to evaluate the effect of high temperature, we measured the zeta-potential of as-made silica spheres (−45.8 ± 3.5 mV) and found that it was greatly reduced for the calcinated silica spheres (−13.6 ± 2.7 mV). Although the zeta-potential of the silica spheres after sintering cannot be measured, it is expected to be further significantly reduced.

Protein Adsorption on Nanopore Surface. Molecular transport in nanopores is strongly affected by the interactions with the nanopore surface.[73] Therefore, it is important to access the extent of protein adsorption on the silica nanopore walls. Protein interactions with silica surfaces have been widely studied[52,74,75] and it is well-known that at physiological pH silica surfaces undergo nonspecific binding of proteins[30,53] with maximum adsorption at pH 5.[76] However, such adsorption is expected to be greatly affected by the high temperature treatment of the silica surface during the sintering process, which leads to the removal of the silanol groups (see above).

To address the possibility of nonspecific protein adsorption onto the silica colloidal crystal nanopores as a factor in transport selectivity, we measured the absorption of the model proteins on calcinated silica nanospheres in solution. We used UV−vis absorbance measurements of dissolved proteins in supernatant aliquots prior to and after stirring with silica spheres under buffer conditions matching those of the diffusion experiments. The silica nanoparticles were removed from the supernatant by centrifugation at speeds that were suitably low so as not to cause sedimentation of the dissolved proteins from solution.

We found that adsorption of all three proteins was rather small for calcinated silica spheres. BHb appeared to adsorb in greater quantities than BSA and Lz, which can be attributed to its larger size than Lz (Table 4). This small extent of protein adsorption is likely the result of the removal of silanol groups by the high temperature treatment, which was indicated by the zeta potential measurements (see above) and by the absence of electrostatic effects on the diffusion. Therefore, the diffusion rates measured in the above experiments are likely not affected by protein adsorption and correspond exclusively to the effects of nanopore size and tortuosity.

Table 4. Amount of Protein Adsorbed onto Silica Surfaces (Initial Protein Concentration = 2.70×10^{-5} M)

protein	mmol protein/g silica ($\times 10^{-4}$)	protein/nm^2
Lz	5.5 ± 0.9	0.04 ± 0.01
BSA	3.0 ± 1.0	0.03 ± 0.01
BHb	10.0 ± 0.8	0.08 ± 0.01

CONCLUSIONS

We studied protein diffusion across sintered silica colloidal crystals with nanopores of various diameters. We demonstrated that these colloidal crystals exhibit size selectivity when the nanopores are sufficiently small (7.5 and 19 nm). Because these nanopores are still larger than the diffusing proteins, the observed size selectivity can be attributed to the tortuosity of the colloidal nanopores. Larger (27 nm) pores led to higher transport rates but at the cost of selectivity. In addition to the size selectivity, we also demonstrated that 19 nm nanopores possess the ability to discriminate biomolecules of comparable molecular weights according to their shape. We also showed that the high temperature sintering required for the preparation of these colloidal crystals leads to reduced interactions between the proteins and the nanopores surface, which appear to play a minor role in the diffusion, with transport selectivity resulting from size and shape effects.

Taken together, our observations suggest that sintered silica colloidal crystals constitute promising nanoporous membranes for protein separations, with easily controllable pore size, size and shape selectivity, and minimal surface fouling. Their selectivity in protein separation is comparable or exceeds that reported for the polymeric and nanotube systems with cylindrical pores of similar diameter, although their flux is lower due to the tortuous pore path and greater thickness of the colloidal membranes prepared in the present work.[18,77,78]

Sintered silica colloidal crystals are mechanically robust and can be easily cut into desired shapes using a CO_2 laser, but the vertical deposition method of their preparation described in the present work limits their size. Nevertheless, the prepared membranes can be incorporated into microfluidic systems (Figure 4), where they might find applications in analytical-scale protein separations. Larger-scale separations would require the development of methods to prepare sintered colloidal crystals with larger areas. This work is underway in our laboratory and will be reported elsewhere.

DOI: 10.1021/acs.langmuir.8b01261
Langmuir 2018, 34, 10333−10339

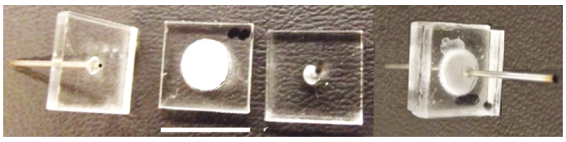

Figure 4. Photographs of sintered silica colloidal crystal membrane incorporated into a microfluidic device. Scale bar is 1 cm.

AUTHOR INFORMATION

Corresponding Author

*E-mail: i.zharov@utah.edu.

ORCID

Ilya Zharov: 0000-0002-6292-8440

Present Address

†P.A.A.I.-d.L.: Energy Systems, Argonne National Laboratory, 9700 S. Cass Avenue, Building 362, Argonne, IL 60439-4844, USA.

Notes

The authors declare no competing financial interest.

ACKNOWLEDGMENTS

This work was supported by the National Science Foundation (CHE-1710052).

REFERENCES

(1) Wong, S.; Kitaev, V.; Ozin, G. A. Colloidal Crystal Films: Advances in Universality and Perfection. *J. Am. Chem. Soc.* **2003**, *125* (50), 15589−15598.

(2) Blanco, A.; Chomski, E.; Grabtchak, S.; Ibisate, M.; John, S.; Leonard, S. W.; Lopez, C.; Meseguer, F.; Miguez, H.; Mondia, J. P.; et al. Large-Scale Synthesis of a Silicon Photonic Crystal with a Complete Three-Dimensional Bandgap near 1.5 Micrometres. *Nature* **2000**, *405* (6785), 437−440.

(3) Bartlett, P. N.; Ghanem, M. A.; El Hallag, I. S.; de Groot, P.; Zhukov, A. Electrochemical Deposition of Macroporous Magnetic Networks Using Colloidal Templates. *J. Mater. Chem.* **2003**, *13* (10), 2596.

(4) Park, S. H.; Xia, Y. Macroporous Membranes with Highly Ordered and Three-Dimensionally Interconnected Spherical Pores. *Adv. Mater.* **1998**, *10* (13), 1045−1048.

(5) Cassagneau, T.; Caruso, F. Semiconducting Polymer Inverse Opals Prepared by Electropolymerization. *Adv. Mater.* **2002**, *14* (1), 34−38.

(6) Peng Lee, K.; Mattia, D. Monolithic Nanoporous Alumina Membranes for Ultrafiltration Applications: Characterization, Selectivity−Permeability Analysis and Fouling Studies. *J. Membr. Sci.* **2013**, *435*, 52−61.

(7) El-Safty, S. a.; Hoa, N. D.; Shenashen, M. a. Topical Developments of Nanoporous Membrane Filters for Ultrafine Noble Metal Nanoparticles. *Eur. J. Inorg. Chem.* **2012**, *2012*, 5439−5450.

(8) Chen, L.; Zhu, G.; Zhang, D.; Zhao, H.; Guo, M.; Shi, W.; Qiu, S. Novel Mesoporous Silica Spheres with Ultra-Large Pore Sizes and Their Application in Protein Separation. *J. Mater. Chem.* **2009**, *19* (14), 2013.

(9) Ke, X. B.; Shao, R. F.; Zhu, H. Y.; Yuan, Y.; Yang, D. J.; Ratinac, K. R.; Gao, X. P. Ceramic Membranes for Separation of Proteins and DNA through in Situ Growth of Alumina Nanofibres inside Porous Substrates. *Chem. Commun.* **2009**, *0* (10), 1264.

(10) Wang, Z.; Le, G.; Shi, Y.; Węgrzyn, G. Purification of Plasmid DNA Using a Multicompartment Electrolyser Separated by Ultrafilter Membranes. *Biotechnol. Lett.* **2002**, *24* (2), 121−124.

(11) Tomanee, P.; Hsu, J. T.; Ito, Y. Preparative Fractionation of Protein, RNA, and Plasmid DNA Using Centrifugal Precipitation Chromatography with Tubular Dialysis Membrane Inside a Convoluted Tubing as Separation Channel. *Biotechnol. Prog.* **2006**, *22* (2), 532−537.

(12) Mohamed, H.; Szarowski, D. H.; Lepak, L. A.; Spencer, M. G.; Martin, D. L.; Caggana, M.; Turner, J. N. Purification of PCR-Inhibitory Components by Cellulose Acetate Membranes. In *NSTI Nanotech, NSTI Nanotechnology Conference and Trade Show*; Laudon, M., Romanowicz, B., Eds.; Anaheim, CA, **2005**; pp 446−448.

(13) Heller, C.; Beck, S. Membrane Electrophoresis of DNA. *Electrophoresis* **1993**, *14* (1), 162−164.

(14) Nge, P. N.; Yang, W.; Pagaduan, J. V.; Woolley, A. T. Ion-Permeable Membrane for on-Chip Preconcentration and Separation of Cancer Marker Proteins. *Electrophoresis* **2011**, *32* (10), 1133−1140.

(15) van Reis, R.; Zydney, A. Bioprocess Membrane Technology. *J. Membr. Sci.* **2007**, *297* (1−2), 16−50.

(16) Wang, J.; Zhu, J.; Zhang, Y.; Liu, J.; Van der Bruggen, B. Nanoscale Tailor-Made Membranes for Precise and Rapid Molecular Sieve Separation. *Nanoscale* **2017**, *9* (9), 2942−2957.

(17) Ulbricht, M. Advanced Functional Polymer Membranes. *Polymer* **2006**, *47* (7), 2217−2262.

(18) Qiu, X.; Yu, H.; Karunakaran, M.; Pradeep, N.; Nunes, S. P.; Peinemann, K. V. Selective Separation of Similarly Sized Proteins with Tunable Nanoporous Block Copolymer Membranes. *ACS Nano* **2013**, *7* (1), 768−776.

(19) Tsapatsis, M. 2-Dimensional Zeolites. *AIChE J.* **2014**, *60* (7), 2374−2381.

(20) Ranjan, R.; Tsapatsis, M. Microporous Metal Organic Framework Membrane on Porous Support Using the Seeded Growth Method. *Chem. Mater.* **2009**, *21* (5), 4920−4924.

(21) Tong, H. D.; Jansen, H. V.; Gadgil, V. J.; Bostan, C. G.; Berenschot, E.; van Rijn, C. J. M.; Elwenspoek, M. Silicon Nitride Nanosieve Membrane. *Nano Lett.* **2004**, *4*, 283−287.

(22) Striemer, C. C.; Gaborski, T. R.; McGrath, J. L.; Fauchet, P. M. Charge- and Size-Based Separation of Macromolecules Using Ultrathin Silicon Membranes. *Nature* **2007**, *445* (7129), 749−753.

(23) Yamaguchi, A.; Uejo, F.; Yoda, T.; Uchida, T.; Tanamura, Y.; Yamashita, T.; Teramae, N. Self-Assembly of a Silica−Surfactant Nanocomposite in a Porous Alumina Membrane. *Nat. Mater.* **2004**, *3* (5), 337−341.

(24) Liu, N.; Dunphy, D. R.; Atanassov, P.; Bunge, S. D.; Chen, Z.; López, G. P.; Boyle, T. J.; Brinker, C. J. Photoregulation of Mass Transport through a Photoresponsive Azobenzene-Modified Nanoporous Membrane. *Nano Lett.* **2004**, *4*, 551−554.

(25) Li, D.; Kaner, R. B. Graphene-Based Materials. *Science (Washington, DC, U. S.)* **2008**, *320* (5880), 1170−1171.

(26) Hinds, B. J.; Chopra, N.; Rantell, T.; Andrews, R.; Gavalas, V.; Bachas, L. G. Aligned Multiwalled Carbon Nanotube Membranes. *Science (Washington, DC, U. S.)* **2004**, *303* (5654), 62−65.

(27) Green, E.; Fullwood, E.; Selden, J.; Zharov, I. Functional Membranes via Nanoparticle Self-Assembly. *Chem. Commun.* **2015**, *51* (37), 7770−7780.

(28) Zharov, I.; Khabibullin, A. Surface-Modified Silica Colloidal Crystals: Nanoporous Films and Membranes with Controlled Ionic and Molecular Transport. *Acc. Chem. Res.* **2014**, *47* (2), 440−449.

(29) Jiang, P.; Bertone, J. F.; Hwang, K. S.; Colvin, V. L. Single-Crystal Colloidal Multilayers of Controlled Thickness. *Chem. Mater.* **1999**, *11* (8), 2132−2140.

(30) Rosen, J. E.; Gu, F. X. Surface Functionalization of Silica Nanoparticles with Cysteine: A Low-Fouling Zwitterionic Surface. *Langmuir* **2011**, *27* (17), 10507−10513.

(31) Stöber, W.; Fink, A.; Bohn, E. Controlled Growth of Monodisperse Silica Spheres in the Micron Size Range. *J. Colloid Interface Sci.* **1968**, *26* (1), 62−69.

(32) Newton, M. R.; Bohaty, A. K.; White, H. S.; Zharov, I. Chemically Modified Opals as Thin Permselective Nanoporous Membranes. *J. Am. Chem. Soc.* **2005**, *127* (20), 7268−7269.

(33) Newton, M. R.; Bohaty, A. K.; Zhang, Y.; White, H. S.; Zharov, I. PH- and Ionic Strength-Controlled Cation Permselectivity in Amine-Modified Nanoporous Opal Films. *Langmuir* **2006**, *22* (9), 4429−4432.

DOI: 10.1021/acs.langmuir.8b01261
Langmuir 2018, 34, 10333−10339

(34) Smith, J. J.; Zharov, I. Ion Transport in Sulfonated Nanoporous Colloidal Films. *Langmuir* **2008**, *24* (6), 2650−2654.
(35) Smith, J. J.; Abbaraju, R. R.; Zharov, I. Proton Transport in Assemblies of Silica Colloidal Spheres. *J. Mater. Chem.* **2008**, *18* (44), 5335.
(36) Bohaty, A. K.; Newton, M. R.; Zharov, I. Light-Controlled Ion Transport through Spiropyran-Modified Nanoporous Silica Colloidal Films. *J. Porous Mater.* **2010**, *17* (4), 465−473.
(37) Cichelli, J.; Zharov, I. Chiral Permselectivity in Surface-Modified Nanoporous Opal Films. *J. Am. Chem. Soc.* **2006**, *128* (25), 8130−8131.
(38) Cichelli, J.; Zharov, I. Chiral Permselectivity in Nanoporous Opal Films Surface-Modified with Chiral Selector Moieties. *J. Mater. Chem.* **2007**, *17* (19), 1870−1875.
(39) Mollard, A.; Ibragimova, D.; Antipin, I. S.; Konovalov, A. I.; Stoikov, I.; Zharov, I. Molecular Transport in Thiacalix[4]Arene-Modified Nanoporous Colloidal Films. *Microporous Mesoporous Mater.* **2010**, *131* (1), 378−384.
(40) Bohaty, A. K.; Smith, J. J.; Zharov, I. Free-Standing Silica Colloidal Nanoporous Membranes. *Langmuir* **2009**, *25* (5), 3096−3101.
(41) Le, T. V.; Ross, E. E.; Velarde, T. R. C.; Legg, M. A.; Wirth, M. J. Sintered Silica Colloidal Crystals with Fully Hydroxylated Surfaces. *Langmuir* **2007**, *23*, 8554−8559.
(42) Bogush, G. H.; Tracy, M. A.; Zukoski, C. F., IV Preparation of Monodisperse Silica Particles: Control of Size and Mass Fraction. *J. Non-Cryst. Solids* **1988**, *104*, 95−106.
(43) Ignacio-de Leon, P. A. a; Zharov, I. Size-Selective Molecular Transport through Silica Colloidal Nanopores. *Chem. Commun. (Cambridge, U. K.)* **2011**, *47* (1), 553−555.
(44) Wang, J.; Liu, B. Fluorescence Resonance Energy Transfer between an Anionic Conjugated Polymer and a Dye-Labeled Lysozyme Aptamer for Specific Lysozyme Detection. *Chem. Commun.* **2009**, *0* (17), 2284−2286.
(45) Zhang, M.; He, X.; Chen, L.; Zhang, Y. Preparation and Characterization of Iminodiacetic Acid-Functionalized Magnetic Nanoparticles and Its Selective Removal of Bovine Hemoglobin. *Nanotechnology* **2011**, *22* (6), 065705.
(46) Chun, K. Y.; Stroeve, P. Protein Transport in Nanoporous Membranes Modified with Self-Assembled Monolayers of Functionalized Thiols. *Langmuir* **2002**, *18* (12), 4653−4658.
(47) Hou, X.; Guo, W.; Jiang, L. Biomimetic Smart Nanopores and Nanochannels. *Chem. Soc. Rev.* **2011**, *40* (5), 2385−2401.
(48) Ileri, N.; Faller, R.; Palazoglu, A.; Létant, S. E.; Tringe, J. W.; Stroeve, P. Molecular Transport of Proteins through Nanoporous Membranes Fabricated by Interferometric Lithography. *Phys. Chem. Chem. Phys.* **2013**, *15* (3), 965−971.
(49) Wu, Z.; Wei, B.; Zhang, X.; Wirth, M. J. Efficient Separations of Intact Proteins Using Slip-Flow with Nano-Liquid Chromatography−Mass Spectrometry. *Anal. Chem.* **2014**, *86* (3), 1592−1598.
(50) Rogers, B. J.; Birdsall, R. E.; Wu, Z.; Wirth, M. J. RPLC of Intact Proteins Using Sub-0.5 Mm Particles and Commercial Instrumentation. *Anal. Chem.* **2013**, *85* (14), 6820−6825.
(51) Chabanov, A. A.; Jun, Y.; Norris, D. J. Avoiding Cracks in Self-Assembled Photonic Band-Gap Crystals. *Appl. Phys. Lett.* **2004**, *84* (18), 3573−3575.
(52) Sang, L.-C.; Vinu, A.; Coppens, M.-O. General Description of the Adsorption of Proteins at Their Iso-Electric Point in Nanoporous Materials. *Langmuir* **2011**, *27* (22), 13828−13837.
(53) Bharti, B.; Meissner, J.; Findenegg, G. H. Aggregation of Silica Nanoparticles Directed by Adsorption of Lysozyme. *Langmuir* **2011**, *27* (16), 9823−9833.
(54) Pujar, N. S.; Zydney, A. L. Electrostatic Effects on Protein Partitioning in Size-Exclusion Chromatography and Membrane Ultrafiltration. *J. Chromatogr. A* **1998**, *796* (2), 229−238.
(55) Chun, K.-Y.; Mafe, S.; Ramírez, P.; Stroeve, P. Protein Transport through Gold-Coated, Charged Nanopores: Effects of Applied Voltage. *Chem. Phys. Lett.* **2006**, *418* (4−6), 561−564.
(56) Leoni, L.; Attiah, D.; Desai, T. A. Nanoporous Platforms for Cellular Sensing and Delivery. *Sensors* **2002**, *2* (3), 111−120.
(57) Cussler, E. L. *Diffusion: Mass Transfer in Fluid Systems*, 2nd ed.; Cambridge University Press: New York, 1997.
(58) Schepelina, O.; Zharov, I. Polymer-Modified Opal Nanopores. *Langmuir* **2006**, *22* (25), 10523−10527.
(59) Schepelina, O.; Zharov, I. PNIPAAM-Modified Nanoporous Colloidal Films with Positive and Negative Temperature Gating. *Langmuir* **2007**, *23* (25), 12704−12709.
(60) Abelow, A. E.; Zharov, I. Poly(l-Alanine)-Modified Nanoporous Colloidal Films. *Soft Matter* **2009**, *5* (2), 457−462.
(61) Schepelina, O.; Poth, N.; Zharov, I. PH-Responsive Nanoporous Silica Colloidal Membranes. *Adv. Funct. Mater.* **2010**, *20* (12), 1962−1969.
(62) Saxton, M. J. Two-Dimensional Continuum Percolation Threshold for Diffusing Particles of Nonzero Radius. *Biophys. J.* **2010**, *99* (5), 1490−1499.
(63) Newton, M. R.; Morey, K. A.; Zhang, Y.; Snow, R. J.; Diwekar, M.; Shi, J.; White, H. S. Anisotropic Diffusion in Face-Centered Cubic Opals. *Nano Lett.* **2004**, *4* (5), 875−880.
(64) Cadman, A. D.; Fleming, R.; Guy, R. H. Diffusion of Lysozyme Chloride in Water and Aqueous Potassium Chloride Solutions. *Biophys. J.* **1982**, *37* (3), 569−574.
(65) Brune, D.; Kim, S. Predicting Protein Diffusion Coefficients. *Proc. Natl. Acad. Sci. U. S. A.* **1993**, *90* (9), 3835−3839.
(66) Gaigalas, A. K.; Hubbard, J. B.; McCurley, M.; Woo, S. Diffusion of Bovine Serum Albumin in Aqueous Solutions. *J. Phys. Chem.* **1992**, *96* (5), 2355−2359.
(67) Torres, J. F.; Komiya, A.; Okajima, J.; Maruyama, S. Measurement of the Molecular Mass Dependence of the Mass Diffusion Coefficient in Protein Aqueous Solutions. *Defect Diffus. Forum* **2012**, *326−328*, 452−458.
(68) Yu, S.; Lee, S. B.; Kang, M.; Martin, C. R. Size-Based Protein Separations in Poly(Ethylene Glycol)-Derivatized Gold Nanotubule Membranes. *Nano Lett.* **2001**, *1* (9), 495−498.
(69) Hart, T. K.; Pino, R. M. Capillary Permeability in the Pancreas and Colon: Restriction of Exogenous and Endogenous Molecules by Fenestrated Endothelia. *Am. J. Anat.* **1986**, *175* (1), 49−58.
(70) Ioffe, V. M.; Gorbenko, G. P.; Kinnunen, P. K. J.; Tatarets, A. L.; Kolosova, O. S.; Patsenker, L. D.; Terpetschnig, E. A. Tracing Lysozyme-Lipid Interactions with Long-Wavelength Squaraine Dyes. *J. Fluoresc.* **2006**, *17* (1), 65−72.
(71) Vansant, E. F.; van der Voort, P.; Vrancken, K. C. *Characterization and Chemical Modification of the Silica Surface*; Elsevier, 1995.
(72) Zhuravlev, L. T. The Surface Chemistry of Amorphous Silica. Zhuravlev Model. *Colloids Surf., A* **2000**, *173* (1−3), 1−38.
(73) Bhatia, S. K.; Bonilla, M. R.; Nicholson, D. Molecular Transport in Nanopores: A Theoretical Perspective. *Phys. Chem. Chem. Phys.* **2011**, *13* (34), 15350−15383.
(74) Hu, H.; Zhou, H.; Du, J.; Wang, Z.; An, L.; Yang, H.; Li, F.; Wu, H.; Yang, S. Biocompatiable Hollow Silica Microspheres as Novel Ultrasound Contrast Agents for in Vivo Imaging. *J. Mater. Chem.* **2011**, *21* (18), 6576.
(75) Holt, P. F.; Bowcott, J. E. Adsorption of Protein on Silica Surfaces. *AMA. Arch. Ind. Hyg. Occup. Med.* **1954**, *9* (6), 503−506.
(76) Du, Y. J.; Brash, J. L. Synthesis and Characterization of Thiol-Terminated Poly(Ethylene Oxide) for Chemisorption to Gold Surface. *J. Appl. Polym. Sci.* **2003**, *90* (2), 594−607.
(77) Ku, J. R.; Stroeve, P. Protein Diffusion in Charged Nanotubes: "On-Off" Behavior of Molecular Transport. *Langmuir* **2004**, *20* (5), 2030−2032.
(78) Nguyen, Q. H.; Ali, M.; Bayer, V.; Neumann, R.; Ensinger, W. Charge-Selective Transport of Organic and Protein Analytes through Synthetic Nanochannels. *Nanotechnology* **2010**, *21* (36), 365701.

DOI: 10.1021/acs.langmuir.8b01261
Langmuir 2018, 34, 10333−10339